Article

Effect of a Phosphorus Additive on Luminescent and Scintillation Properties of Ceramics GYAGG:Ce

Lydia V. Ermakova [1], Valentina G. Smyslova [1], Valery V. Dubov [1], Daria E. Kuznetsova [1], Maria S. Malozovskaya [1], Rasim R. Saifutyarov [1], Petr V. Karpyuk [1], Petr S. Sokolov [1,*], Ilia Yu. Komendo [1], Aliaksei G. Bondarau [2], Vitaly A. Mechinsky [2] and Mikhail V. Korzhik [2]

[1] National Research Center "Kurchatov Institute", 123098 Moscow, Russia; ermakova.lydia@gmail.com (L.V.E.); smyslovavg@gmail.com (V.G.S.); valery_dubov@mail.ru (V.V.D.); daria_kyznecova@inbox.ru (D.E.K.); puellamay@mail.ru (M.S.M.); rosya01@gmail.com (R.R.S.); silancedie@mail.ru (P.V.K.); i.comendo@gmail.com (I.Y.K.)
[2] Institute for Nuclear Problems, Belarus State University, 220030 Minsk, Belarus; alesonep@gmail.com (A.G.B.); vitaly.mechinsky@cern.ch (V.A.M.); mikhail.korjik@cern.ch (M.V.K.)
* Correspondence: sokolov-petr@yandex.ru

Abstract: The production of the scintillation ceramics can require the utilization of the phosphorus compounds at certain stages of 3D-printing, such as vat polymerization, applied for the formation of green bodies before sintering. The effect of phosphorus additive on the microstructure, optical, and scintillation parameters of $Gd_{1.494}Y_{1.494}$ $Ce_{0.012}Al_2Ga_3O_{12}$ (GYAGG:Ce) ceramics obtained by pressureless sintering at 1650 °C in an oxygen atmosphere was investigated for the first time. Phosphorus was introduced in the form of $NH_4H_2PO_4$ into the initial hydroxocarbonate precipitate in a wide concentration range (from 0 to 0.6 wt.%). With increasing of phosphorus concentration, the density and the optical transmittance of garnet ceramics show a decrease, which is caused by an increase in the number of pores and inclusions. The light yield of fast scintillation, which is caused by Ce^{3+} ions, was found to be affected by the phosphorus additive as well. Moreover, an increase in phosphorescence intensity was recognized.

Keywords: ceramics; garnet; phosphorus; luminescence; phosphorescence; stereolithography

1. Introduction

Garnet structure oxides doped with lanthanides are a group of widely used luminescent, laser and scintillation materials [1–15]. $Y_3Al_5O_{12}$:Ce (YAG:Ce) and $Lu_3Al_5O_{12}$:Ce (LuAG:Ce) are well-established scintillators, which are widely used in radiation detection applications in science and industry. Nevertheless, recently, along with binary compositions, such as YAG:Ce and LuAG:Ce, multicationic garnets have been actively studied [1–3,5–9]. The garnet matrix is developed to become more complex; yttrium is partially or completely replaced by gadolinium or a Gd/Lu mixture in different ratios; and aluminum is partially replaced by gallium [8–11]. In addition, garnets doped with other lanthanides, or their combination are being actively studied [1,5–7,12]. Compositionally disordered garnet structure compounds with a general formula $(Gd,Y,Lu)_3(Al,Ga)_5O_{12}$, doped with rare earth activator(s) and, facultatively co-doped with other element(s) became in the focus of the research due to a unique set of features: high chemical stability, high density, high effective atomic number, high light yield, fast scintillation kinetics, etc. [6,8–10,15–17]. It can be produced in the form of both single crystals [9,10,16–18] and translucent [15] or transparent ceramics [8,10,13,19].

Luminescent ceramics have some advantages in comparison to single crystals of the same structure and composition. Ceramics can be produced more cheaply, potentially any shape, almost any size and/or composition. Also, new structures are accessible due to the

versatility of ceramics, e.g., composites [20–23]. At the same time, the major functional properties of highly transparent ceramics could be over to single crystals.

Various additive manufacturing techniques were applied to produce transparent [22,23] or translucent [24,25] garnet ceramics. Material jetting [22] and direct ink write [23] methods were used for the formation of green body further used for the sintering. YAG:Yb/YAG:Nd and YAG:Er/YAG:Lu transparent all-ceramic composites of disk-like [22] or rod-like [23] shapes were obtained by vacuum/air sintering with subsequent hot isostatic pressing. Also new methods for sintering garnet ceramics under electron-beam [26] and laser [27] irradiation seem promising. Nevertheless, one of the most frequently developed methods of 3D-printing suitable for mass applications, is stereolithography. It provides one of the best spatial resolutions, a smooth surface of printed objects with an acceptable building speed and a possibility to use the pressureless sintering [24,25].

Obviously, the key properties of garnet ceramics depend on the chemical composition and the perfection of the oxide matrix [12,14,15], the chosen activators [28–31], technological factors [19,30–33], synthesis conditions [8] and post-processing treatment [31]. Another important factor is the nature and a concentration of impurities which come in the ceramics at different stages of the technology. There are a plenty of publications describing the influence of cations of various metals, such as alkali [32] and alkaline earth elements [9,16,17,31,33,34], elements of the third [18,20] and fourth [34] groups. The effect of silicon [22,23,33–35] and boron [33,36] additives has been also well clarified. Silicon is a widely used sintering additive [[33] and refs therein], which is utilized to prepare transparent or translucent garnet ceramics. The disadvantage of using such sintering additives is their potential negative effects on the luminescent and scintillation properties of the resulting ceramics [32,33,36].

Research on the influence of other non-metals, such as nitrogen, is much less described [35]. Phosphorus is a typical non-metal element, a neighbor of nitrogen and silicon in the periodic table. However, to the best of our knowledge, the effect of phosphorus additives on garnet ceramics has not been practically studied before. Only single article has been recently published, where YPO_4/YAG:Ce nanocomposites were purposefully synthesized and studied in details [37]. At the same time, it is well known that phosphorus-containing dispersants can be used in the preparation of slurries in ceramic technology [38,39], including slurries for 3D-printing. Phosphoric acid ester derivatives have high wetting characteristics for surface oxide powders. It allows to reach a high loading of slurries with acceptable rheological properties [38,39]. The typical value of specific surface area (SSA) is from 45 to 60 m^2/g and from 3 to 12 m^2/g, for garnet oxide powders annealed at 850 and 1300 °C [24,25], respectively. The content of the dispersant in slurry is usually proportional to the SSA of the ceramic powder and can be reached up to 3 mg for each m^2 [24,25]. According to our preliminary study, the phosphorus content in commercially available dispersants is about 4 wt.%.

Moreover, UV photocurable slurries with ceramic particles for stereolithography 3D printing may contain other phosphorus compounds, like UV photoinitiators of radical polymerization of the class of phosphine oxides (BAPO, TPO, TPO-L, etc.). The typical content of such photoinitiators is ~1.0 wt.% based on the weight of acrylate monomers [24,25]. Thus, the potential content of phosphorus in the slurry can be quite high value (1–7 mg for each g of powder or 1000–7000 ppm). The high sintering temperature could induce the partial volatilization of phosphorus, which may result in loose microstructure of garnet ceramics. The formation of impurity phases is also very possible.

Here, we report for the first time an effect of phosphorus impurity on major function properties of doped with GYAGG:Ce garnet scintillation ceramics. The key properties of the sintered ceramics were correlated with the amount of phosphorus.

2. Materials and Methods

2.1. Synthesis of Initial Powders

Starting powder was fabricated by co-precipitation method [5–7,11–13,33]. High purity commercially available chemical reagents such as Gd_2O_3 (99.995%), Y_2O_3 (99.995%),

AlOOH (99.998%), Ga (99.999%) and $Ce(NO_3)_3$ (99.95%) were used as raw materials to prepare nitrate solutions. The solutions were mixed in the required proportions to obtain composition $Gd_{1.494}Y_{1.494}Ce_{0.012}Al_2Ga_3O_{12}$ and diluted to obtain the total Me^{3+} ion concentration of 0.5 mol/L. Next, the mixed solution was slowly added to the precipitant—a solution of ammonium bicarbonate NH_4HCO_3 (99.95%) with a concentration of 1.5 mol/L, under constant stirring with an overhead stirrer. The hydroxocarbonate precipitate was filtered, washed with high-purity isopropyl alcohol (IPA)—distillated water mixture a few times, and dried at 80 °C in air ventilated oven for 8 h. Further, the precipitate was divided into four equal parts. One part was used as a reference (untreated) sample, the other three parts were utilized to enhance the phosphorus content.

The $NH_4H_2PO_4$ (99.5%) was used as a source of phosphorus, the details of introducing are described elsewhere [33]. Three IPA-water solutions with different concentration of phosphorus were prepared. Weighed portion of the precipitate was added in each solution. These suspensions were stirred for a day, then dried at 80 °C, and samples were taken for elemental analysis. The motivation of choosing this substance as a source of phosphorus is presented in the Supplementary.

Finally, all four precursors with different phosphorus content were placed in corundum crucibles with caps and calcined together in a muffle furnace at 850 °C for 2 h to form the garnet phase. During annealing, the precipitate showed a weight loss of about 29%. Afterward, the oxide powders were milled in a planetary ball mill with alumina jars and beads to get a median particle size (d_{50}) of 1.5–1.8 μm according to laser diffraction measurements. The grinding conditions were identical for all compositions. Milling media was IPA, rotation speed was 300 rpm; grinding time was 30 min, weight ratio of IPA:powder:beads was 2:1:2. After milling the slurries were dried at 80 °C and sieved through a 100-μm meshes. Samples were taken for elemental analysis. As the result, four samples: nominally pure (#0) and, loaded with phosphorus (#1–3) were produced. The stages of their production and characterization methods are described below.

2.2. Characterization of Initial Powders

Particle size distributions were measured using laser diffraction on a MasterSizer 2000 (Malvern, PA, USA) with a water-filled dispersing unit Hydro G. The specific surface area (SSA) and pore volume of the powders were determined according to the capillary nitrogen condensation method using BET and BJH models on NOVAtouch NT LX (Quantachrome Instruments, New York, NY, USA). The phase compositions of the oxide powders were examined using X-ray powder diffraction on a D2 Phaser (Bruker, Billerica, MA, USA) with $CuK\alpha_{1,2}$ radiation.

Elemental analysis of precipitates and calcined powders was carried out via iCAP 6300 duo (Thermo Scientific, Waltham, MA, USA) spectrometer by ICP AES method. Before the measurement, the powders are dissolved in a mixture of ultra-pure nitric and hydrochloric acids at temperature of 100 °C using a HotBlock (Environmental express, Ocala, FL, USA) equipment.

2.3. Ceramics Fabrication

Green bodies were prepared by uniaxial pressing at 64 MPa into 1.5 mm-thick pellets of 20 mm in diameter. The typical green density was about 35% of the theoretical density of a single-crystal GYAGG:Ce (6.0 g/cm³). Then pellets were sintered at 1650 °C 2 h in an oxygen atmosphere by using tube furnace.

Finally, surface of the ceramic samples was grinded with silicon carbide abrasive papers and then polished with 0.5 μm and 0.1 μm diamond polishing pastes. The thickness of the ceramic samples was ~1 mm. The polished samples intended for scanning electron microscopy were additionally thermally etched for 10 min at 1200 °C to reveal grain boundaries.

2.4. Characterization of Ceramic Samples

The apparent density of the ceramic samples was measured using Archimedes' method in Lotoxane at room temperature. The uncertainty in this measurement was about 0.5%.

Ceramic microstructure was studied using a Jeol JSM-7100F (JEOL, Tokyo, Japan) scanning electron microscope (SEM). SEM images were obtained in secondary electrons and backscattered electrons modes. Platinum sputter-coating was used to ensure electrical conductivity of surface ceramic sample. Local chemical compositions were estimated using energy-dispersive X-ray spectroscopy (EDX) via X-Max 50 (Oxford Instruments, London, UK) attachment. Processing of the SEM images to determine the average grain sizes and estimate of the number of inclusions of ceramics was carried out using ImageJ software.

The full transmittance of the ceramic samples in the visible region of the spectrum (400–700 nm) was determined on an Specord Plus spectrophotometer (Analytik Jena, Jena, Germany) equipped with an integrating sphere. The photoluminescence (PL) spectra of the ceramic samples were measured on a Fluorat-02 Panorama spectrofluorimeter (Lumex, Moscow, Russia) with a xenon lamp excitation at room temperature.

The photoluminescence kinetics were studied on a FluoTime 250 luminescence spectrometer (PicoQuant, Berlin, Germany) using a pulsed LED excitation source with a wavelength of 340 nm and a pulse width of 200 ps, corresponding to excitation of the $4f \rightarrow 5d_1$ interconfigurational transition of Ce^{3+} ions.

The light output (LO) of the samples was measured with a [137]Cs (662 keV) source by collecting the pulse height spectra with the XP2020 photomultiplier readout. Incident γ-quanta interact with a whole volume of the sample, so the position of the γ-quanta photo-absorption peak in the spectra is affected by the scattering of the scintillation light. Therefore, the light output is smaller than the light yield (LY) due to the reduced light collection factor in the translucent sample.

A thin layer of the sample, not more than 10 µm, absorbs α-particles in the material. Due to this reason, measurement with α-particles in a 45° geometry [40] provides a light yield of scintillation practically from the surface of the sample, which is not affected by scattering. An α-particle source (~5.5 MeV, [241]Am) was used to collect the pulse height spectra with the XP2020 photomultiplier readout. A YAG:Ce single-crystal with ground surfaces to mimic ceramics with a light yield of 4100 ph/MeV under α-particles excitation and 25,000 ph/MeV under γ-quanta excitation was used in these measurements as a reference.

3. Results

The results of quantitative elemental analysis of the phosphorus content in the initial powders are presented in Table 1. Sample # 1 contains approximately Ce 1:1 P (mole ratio).

Table 1. The measurement contents of phosphorus in initial powders (wt.%) [1].

Sample #	Hydroxocarbonate Precipitates	Oxide Powders Calcined at 850 °C
0	-	-
1	0.027	0.040
2	0.114	0.156
3	0.456	0.623

[1] According to elemental analysis, the content of cerium in the hydroxocarbonate precipitates and powders calcined at 850 °C is 0.139(1) and 0.191(1) wt.%, respectively, in good agreement with to the expected chemical composition.

It is known [41,42] that ammonium dihydrogen phosphate completely decomposes into gaseous products already at temperatures of about 550 °C. In the same time, based on the results of elemental analysis, we do not observe significant loss (volatilization) of phosphorus. One can assume that as-synthesized ReE (Y, Gd, Ce) oxides may easy

react with $NH_4H_2PO_4$ [37,43,44] at relatively low temperature and form the refractory and extremely stable phosphates [37,45,46].

The BET specific surface area and the BJH porosity for garnet powder calcined at 850 °C were 55 m^2/g and 0.3 cm^3/g, respectively. According to X-ray diffraction analysis all initial powders had a garnet crystal structure *Ia-3d* with lattice parameter *a* = 12.232(5) Å in good agreement with the literature [7].

Diffractograms of ceramics obtained from sample # 2 and # 3 contain a few additional weak lines, which can be attributed to $(Y,Gd)PO_4$ with a tetragonal (*I4₁/amd*) xenotime structure (Figure S1). Lines of monazite-type phosphates (typical for pure $GdPO_4$) are not observed. The resulting ceramic samples had a high density from 100 to 97.5% (Table 2).

Table 2. The average relative density of GYAGG:Ce ceramic samples (%).

Sample #	0	1	2	3
Relative density	100	99.7	98.8	97.5

Thus, the sinterability and densification of garnet powders with phosphorus are apparently decreased. This behavior can be explained by two factors. Firstly, the presence of an impurity of refractory orthophosphate possibly reduces the sinterability due to high melting point of $YPO_4{\sim}2150$ °C [46], which is higher than the melting point of YAG or GAGG compounds [24]. Secondly, the density of yttrium orthophosphate is significantly lower than the density of GYAGG:Ce ceramics (4.27 vs. 6.0 g/cm^3).

The assumptions above are supported by the electron microscopy data (Figure 1). According to SEM analysis, the grains sizes for GYAGG:Ce ceramics without phosphorus (sample # 0) are up to 7 μm; generally the sample # 0 has a homogeneous microstructure, which is typical for dense garnet ceramics [7,8,13,14,33]. According to the EDX analysis, the element content (Gd 28 wt.%; Y 16 wt.%; Al 6 wt.%; Ga 25 wt.%; O~24 wt.%; Ce 0.2 wt.%) was in good agreement with the synthesized composition. Just few pores and inclusions have been observed. Total amount of inclusions and pores is 0.1(1)% (Table 3).

Table 3. The average grain size of garnet phase, total fraction of inclusions and pores in the GYAGG:Ce ceramic samples.

Sample #	0	1	2	3
Average grain size (μm)	1.90 (1)	3.2 (2)	6.9 (2)	2.8 (2)
Fraction of inclusions + pores (%)	0.1 (1)	0.9 (5)	3.5 (5)	16.3 (9)

All the samples contain a number of pores with different shapes and sizes up to 3–5 μm, which progressively increases in number from 1 to 3 series. The number of impurity grains increases with phosphorus increase in the samples (Figure 1, Table 3) as well. The chemical composition of these grains is slightly variable, in any case they are enriched in phosphorus (up to 12 wt%) and gadolinium (up to 43 wt.%), and depleted in aluminum (down to 1 wt.%) and gallium (down to 3 wt.%), and the same time the yttrium content reaches the 12 wt.%. So, from the comparison of Figure 1d–f, we can conclude that the nature of the main inclusions in sample # 3 are phosphates, in good agreement with our X-ray diffraction data and results from [37].

In samples # 2 and # 3 there are also grains of aluminum-gallium oxide. Earlier, appearance of the $(Al,Ga)_2O_3$ oxide phase was observed when Gd content was below the stoichiometric garnet composition [14]. But in this work, their appearance is explained by the fact that some of the yttrium and gadolinium atoms bind to inert phosphates.
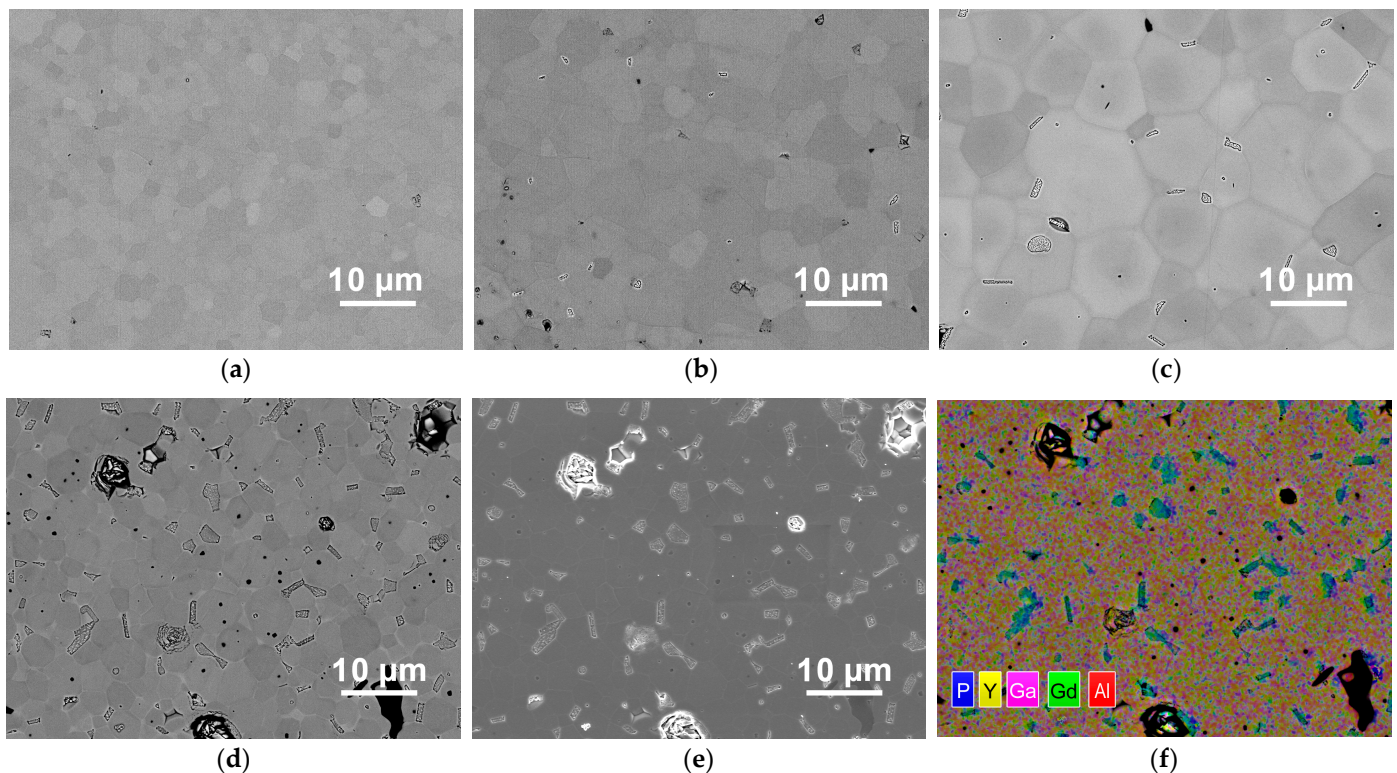
Figure 1. Representative SEM images of mirror polished and thermally etched surfaces of GYAGG:Ce ceramics. (**a**) sample # 0; (**b**) sample # 1; (**c**) sample # 2; (**d**–**f**) sample # 3 (maximum phosphorus content). Sample # 0 is a reference ceramic without phosphorus additives; in other samples, the phosphorus content increases with increasing number. SEM images (**a**–**d**) recorded in backscattered electrons mode and (**e**) recorded in secondary electrons mode; (**f**) element mapping for sample # 3. Scale bar 10 μm.

The average grain size of GYAGG:Ce ceramics without phosphorus (sample # 0) is 1.9 μm. An increase in the average grain size with an increase in the phosphorus concentration in the garnet ceramics was found for sample 0, 1 and 2 (Table 3). The larger grains were observed in sample # 2 (Figure 1c). The average grain size for sample # 3 is 2.8 μm. It is possible that relatively small amounts of phosphorus lead to more active grain growth due to increase in the defectiveness of the garnet structure. And in the case of an excess of phosphorus (sample # 3), impurity phases come out in the form of individual crystallites and have less effect on grain growth.

Optical photographs and additional SEM images (secondary electrons mode) of the ceramic samples are presented in Supplementary as Figures S2 and Figure S3, respectively.

The photoluminescent properties of ceramics are shown in Figure 2. Photoluminescence (PL) and photoexcitation spectra (PLE) of GYAGG:Ce ceramics with phosphorus additives have the characteristic luminescence bands of Ce^{3+} in garnet matrices.

The peak position of the luminescence spectra does not depend on the concentration of phosphorus, while for the excitation spectra, a shift of the excitation band maximum corresponding to the f^1d^0-f^05d^1 transition is observed: from 430 nm for sample # 0 to 450 nm for sample # 3. Worth noting, the luminescence intensity increases with the increasing of phosphorus concentration, passing through a maximum for sample # 2, after which it decreases when passing to sample # 3.

The LO of the ceramic samples correlates with their translucence. Changes in the LO and optical transmission at 520 nm, which correspond to the maximum of the scintillation spectrum, are shown in Figure 3. It is worth stating that there is a clear deterioration of the LO with the transmittance reducing.
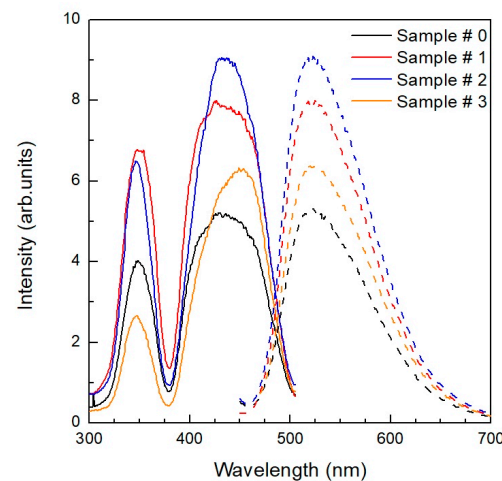
Figure 2. Room temperature measured luminescence (λ_{ex} = 350 nm) and its excitation spectra (λ_{reg} = 520 nm) of GYAGG:Ce ceramics. Number of the series is indicated. Solid lines are PLE spectra; Dashed lines are PL spectra.
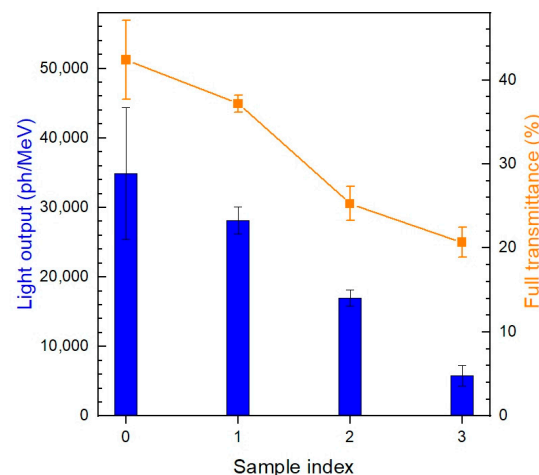

Figure 3. Change of the light output and optical transmittance at 520 nm in the GYAGG:Ce ceramics samples having different concentration of phosphorus. Samples indexes are indicated in Table 1.

Figure 4 shows the pulse height spectra of samples measured upon excitation by alpha particles. The position of the total absorption peak correlates with the scintillation yield of the sample. The positions of the total absorption peaks are as follows: YAG:Ce reference (208 ch.); #0 (331 ch); #1 (306 ch); #2 (261 ch); and #3—no resolved peak at all. Thus, there is a progressive decrease in the LY caused by the fast scintillation of Ce^{3+} ions as the phosphorus concentration increases in the sample. Moreover, scintillation was practically suppressed at the highest phosphorus concentration.

The photoluminescence kinetics of the samples from different series are compared in Figure 5. There is a progressive shortening of the initial stage of the kinetics curve with increasing phosphorus concentration, which indicates quenching of the photoluminescence of Ce^{3+} ions. This process contributes to the decrease in scintillation light yield. But this is not the only process of deterioration; most likely, phosphorus creates a deep electron trapping center, which competes with Ce^{3+} ions to catch non-equilibrium carriers and, at its thermal ionization, provides phosphorescence. This suggestion is supported by an increase in the intensity of the plateau in Figure 5b after the fast photoluminescence stage, which indicates a significant increase in the phosphorescence in the emitting light.
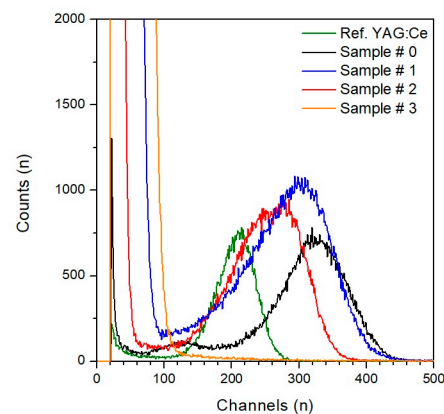
Figure 4. Pulse-height spectra of garnet ceramics and reference YAG:Ce samples measured under α-particles.
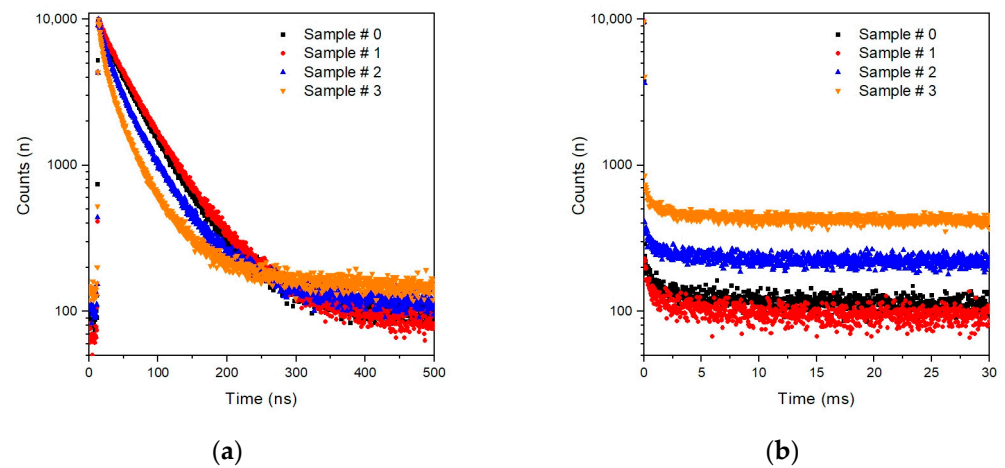

Figure 5. Room temperature PL kinetics of the of GYAGG:Ce ceramic samples at λ_{reg} = 550 nm and excitation λ_{ex} = 340 nm: (**a**)—in a typical time scale applied for Ce^{3+} luminescence kinetics measurements; (**b**)—in a millisecond's scale, which is suitable to observe phosphorescence.

Figure 6 demonstrates the intensity of the persistent luminescence, which intensity is progressively increased in the samples as the phosphorus concentration increases. Persistent luminescence on the second time scale or longer is clearly observed.
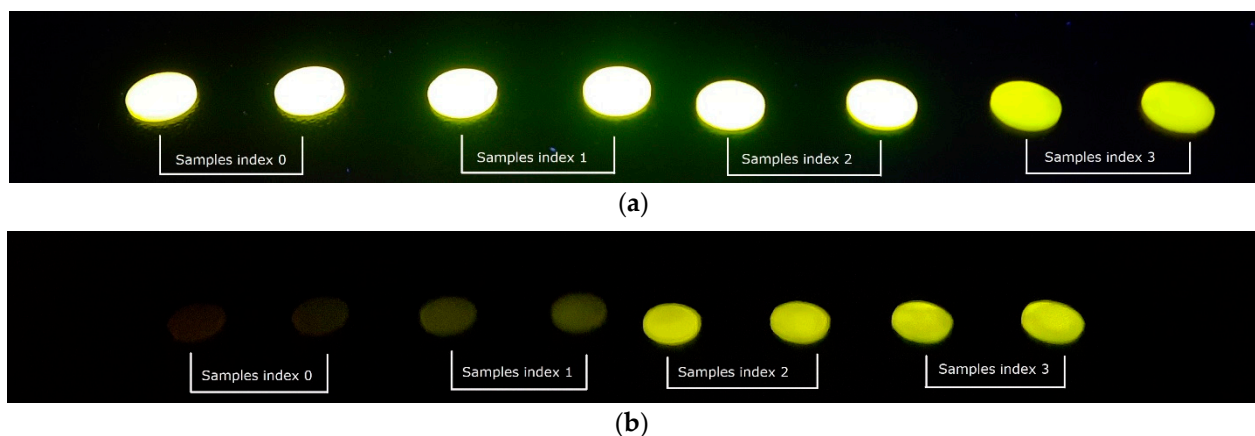
Figure 6. Images of ceramic samples of different series under UV illumination of mercury lamp (λ = 254 nm) (**a**) and 10 s after switch-off the lamp (**b**). Intensity of the persistent luminescence correlates with an increase of the phosphorus in the sample.

4. Discussion

The effect of phosphorus additives on the optical and physical properties of garnet ceramics was found to be quite strong. Apparently, it is due to the relatively high chemical activity of the as-synthesized oxide powders from the hydroxocarbonate precipitate. Phosphorus chemically binds the rare earth elements (Y, Gd, Ce) into inert orthophosphate. As a result, during the process of creating garnet ceramics, a depletion in the concentration of rare earth elements relative to their stoichiometric composition occurs, *viz.*, the phosphates should form second phases (inclusions) in the garnet-type oxides. Recently, the localization of phosphate with respect to cerium luminescence centers in the YAG host has been evaluated by high-resolution scanning transmission electron microscopy and shows distinct YPO_4 and YAG phases in nanocomposite [37]. Based on crystal chemistry, the incorporation of phosphorus into the garnet structure is practically impossible. Indeed, phosphorus contents do not exceed 1 wt% P_2O_5 in garnet minerals [47,48] and mostly as inclusions. To the best of our knowledge, in literature there is just one example, when phosphate forms the garnet crystal structure. To achieve this, a very extreme synthesis conditions were required. The $Na_3Al_2(PO_4)_3$ compound with garnet-like crystal structure and its solid solutions were synthesized at high-pressure (>15 GPa) and high-temperature (>1200 °C) conditions [49]. So, under ambient pressure phosphates will form a separate phase(s).

Thus, governing the amount of phosphorus in the initial reagents and throughout the whole process of making ceramics is an important issue. Even a trace concentration of phosphorus in the ceramics results in an increase in phosphorescence. As a result, such parameters of the scintillation material as afterglow will suffer.

5. Conclusions

For the first time we systematically studied of phase compositions, microstructure, and optical properties of GYAGG:Ce scintillation ceramics with different amounts of phosphorus additives. It is supposed to be important in view of the utilization of the phosphorus chemicals in 3D printing for the precursor densification. Major characteristics of GYAGG:Ce ceramics were found to depend on the amount of phosphorus additives. With increasing phosphorus, the number of defects in the ceramics (pores, secondary phases) increases drastically. Optical transmittance, density, and scintillation yield under alpha- and gamma-excitation are systematically decreased. Phosphorescence intensity shows significant growth as well. All these circumstances require governing the amount of phosphorus in the initial reagents and throughout the whole process of making ceramics.

Conflicts of Interest: The authors declare no conflict of interest.

References

1. Ueda, J.; Tanabe, S. Review of luminescent properties of Ce^{3+}-doped garnet phosphors: New insight into the effect of crystal and electronic structure. *Opt. Mater. X* **2019**, *1*, 100018. [CrossRef]
2. Xia, Z.; Meijerink, A. Ce^{3+}-Doped garnet phosphors: Composition modification, luminescence properties and applications. *Chem. Soc. Rev.* **2017**, *46*, 275–299. [CrossRef] [PubMed]
3. Wu, J.L.; Gundiah, G.; Cheetham, A.K. Structure–property correlations in Ce-doped garnet phosphors for use in solid state lighting. *Chem. Phys. Lett.* **2007**, *441*, 250–254. [CrossRef]
4. Palashov, O.V.; Starobor, A.V.; Perevezentsev, E.A.; Snetkov, I.L.; Mironov, E.A.; Yakovlev, A.I.; Balabanov, S.S.; Permin, D.A.; Belyaev, A.V. Thermo-optical studies of laser ceramics. *Materials* **2021**, *14*, 3944. [CrossRef] [PubMed]
5. Korjik, M.; Bondarau, A.; Dosovitskiy, G.; Dubov, V.; Gordienko, K.; Karpuk, P.; Komendo, I.; Kuznetsova, D.; Mechinsky, V.; Pustovarov, V.; et al. Lanthanoid-doped quaternary garnets as phosphors for high brightness cathodoluminescence-based light sources. *Heliyon* **2022**, *8*, E10193. [CrossRef] [PubMed]
6. Korzhik, M.; Abashev, R.; Fedorov, A.; Dosovitskiy, G.; Gordienko, E.; Kamenskikh, I.; Kazlou, D.; Kuznecova, D.; Mechinsky, V.; Pustovarov, V.; et al. Towards effective indirect radioisotope energy converters with bright and radiation hard scintillators of $(Gd,Y)_3Al_2Ga_3O_{12}$ family. *Nucl. Eng. Technol.* **2022**, *54*, 2579–2585. [CrossRef]
7. Korzhik, M.; Borisevich, A.; Fedorov, A.; Gordienko, E.; Karpyuk, P.; Dubov, V.; Sokolov, P.; Mikhlin, A.; Dosovitskiy, G.; Mechinsky, V.; et al. The scintillation mechanisms in Ce and Tb doped $(Gd_xY_{1-x})Al_2Ga_3O_{12}$ quaternary garnet structure crystalline ceramics. *J. Lumin.* **2021**, *234*, 117933. [CrossRef]
8. Retivov, V.; Dubov, V.; Komendo, I.; Karpyuk, P.; Kuznetsova, D.; Sokolov, P.; Talochka, Y.; Korzhik, M. Compositionally disordered crystalline compounds for next generation of radiation detectors. *Nanomaterials* **2022**, *12*, 4295. [CrossRef]
9. Martinazzoli, L.; Nargelas, S.; Bohacek, P.; Cala, R.; Dusek, M.; Rohlicek, J.; Tamulaitis, G.; Auffray, E.; Nikl, M. Compositional engineering of multicomponent garnet scintillators: Towards an ultra-accelerated scintillation response. *Mater. Adv.* **2022**, *3*, 6842–6852. [CrossRef]
10. Zhu, D.; Nikl, M.; Chewpraditkul, W.; Li, J. Development and prospects of garnet ceramic scintillators: A review. *J. Adv.Ceram.* **2022**, *11*, 1825–1848. [CrossRef]
11. Korzhik, M.; Retivov, V.; Dosovitskiy, G.; Dubov, V.; Kamenskikh, I.; Karpuk, P.; Komendo, I.; Kuznetsova, D.; Smyslova, V.; Mechinsky, V.; et al. First Observation of the Scintillation Cascade in Tb^{3+}-Doped Quaternary Garnet Ceramics. *Phys. Status Solidi R* **2023**, *17*, 2200368. [CrossRef]
12. Karpyuk, P.; Korzhik, M.; Fedorov, A.; Kamenskikh, I.; Komendo, I.; Kuznetsova, D.; Leksina, E.; Mechinsky, V.; Pustovarov, V.; Smyslova, V.; et al. The Saturation of the Response to an Electron Beam of Ce- and Tb-Doped GYAGG Phosphors for Indirect β-Voltaics. *Appl. Sci.* **2023**, *13*, 3323. [CrossRef]
13. Dubov, V.; Gogoleva, M.; Saifutyarov, R.; Kucherov, O.; Korzhik, M.; Kuznetsova, D.; Komendo, I.; Sokolov, P. Micro-Nonuniformity of the Luminescence Parameters in Compositionally Disordered GYAGG:Ce Ceramics. *Photonics* **2023**, *10*, 54. [CrossRef]
14. Retivov, V.; Dubov, V.; Kuznetsova, D.; Ismagulov, A.; Korzhik, M. Gd^{3+} content optimization for mastering high light yield and fast $Gd_xAl_2Ga_3O_{12}$:Ce^{3+} scintillation ceramics. *J. Rare Earths* **2023**, in press. [CrossRef]
15. Kuznetsova, D.; Dubov, V.; Bondarev, A.; Dosovitskiy, G.; Mechinsky, V.; Retivov, V.; Kucherov, O.; Saifutyarov, R.; Korzhik, M. Tailoring of the Gd–Y–Lu ratio in quintuple $(Gd, Lu, Y)_3Al_2Ga_3O_{12}$:Ce ceramics for better scintillation properties. *J. Appl. Phys.* **2022**, *132*, 203104. [CrossRef]
16. Dantelle, G.; Boulon, G.; Guyot, Y.; Testemale, D.; Guzik, M.; Kurosawa, S.; Kamada, K.; Yoshikawa, A. Research on Efficient Fast Scintillators: Evidence and X-Ray Absorption Near Edge Spectroscopy Characterization of Ce^{4+} in Ce^{3+}, Mg^{2+}-Co-Doped $Gd_3Al_2Ga_3O_{12}$ Garnet Crystal. *Phys. Status Solidi B* **2020**, *257*, 1900510. [CrossRef]
17. Korzhik, M.; Alenkov, V.; Buzanov, O.; Dosovitskiy, G.; Fedorov, A.; Kozlov, D.; Mechinsky, V.; Nargelas, S.; Tamulaitis, G.; Vaitkevicius, A. Engineering of a new single-crystal multi-ionic fast and high-light-yield scintillation material $(Gd_{0.5}–Y_{0.5})_3Al_2Ga_3O_{12}$:Ce,Mg. *CrystEngComm* **2020**, *22*, 2502–2506. [CrossRef]
18. Spassky, D.; Kozlova, N.; Zabelina, E.; Kasimova, V.; Krutyak, N.; Ukhanova, A.; Morozov, V.A.; Morozov, A.V.; Buzanov, O.; Chernenko, K.; et al. Influence of the Sc cation substituent on the structural properties and energy transfer processes in GAGG:Ce crystals. *CrystEngComm* **2020**, *22*, 2621–2631. [CrossRef]

19. Shi, Y.; Shichalin, O.; Xiong, Y.; Kosyanov, D.; Wu, T.; Zhang, Q.; Wang, L.; Zhou, Z.; Wang, H.; Fang, J.; et al. Ce^{3+} doped $Lu_3Al_5O_{12}$ ceramics prepared by spark plasma sintering technology using micrometre powders: Microstructure, luminescence, and scintillation properties. *J. Eur. Ceram. Soc.* **2022**, *42*, 6663–6670. [CrossRef]

20. Kuznetsov, S.V.; Sedov, V.S.; Martyanov, A.K.; Batygov, S.C.; Vakalov, D.S.; Boldyrev, K.N.; Tiazhelov, I.A.; Popovich, A.F.; Pasternak, D.G.; Bland, H.; et al. Cerium-doped gadolinium-scandium-aluminum garnet powders: Synthesis and use in X-ray luminescent diamond composites. *Ceram. Int.* **2022**, *48*, 12962–12970. [CrossRef]

21. Fedorov, A.; Komendo, I.; Amelina, A.; Gordienko, E.; Gurinovich, V.; Guzov, V.; Dosovitskiy, G.; Kozhemyakin, V.; Kozlov, D.; Lopatik, A.; et al. GYAGG/^{6}LiF composite scintillation screen for neutron detection. *Nucl. Eng. Technol.* **2022**, *54*, 1024–1029. [CrossRef]

22. Rudzik, T.J.; Seeley, Z.M.; Drobshoff, A.D.; Cherepy, N.J.; Wang, Y.; Onorato, S.P.; Squillante, M.R.; Payne, S.A. Additively manufactured transparent ceramic thin disk gain medium *Opt. Mater. Express.* **2022**, *12*, 3648–3657. [CrossRef]

23. Osborne, R.A.; Wineger, T.J.; Yee, T.D.; Cherepy, N.J.; Seeley, Z.M.; Gaume, R.; Dubinskii, M.; Payne, S.A. Fabrication of engineered dopant profiles in Er/Lu:YAG transparent laser ceramics via additive manufacturing. *Opt. Mater. Express.* **2023**, *13*, 526–537. [CrossRef]

24. Ermakova, L.V.; Dubov, V.V.; Saifutyarov, R.R.; Kuznetsova, D.E.; Malozovskaya, M.S.; Karpyuk, P.V.; Dosovitskiy, G.A.; Sokolov, P.S. Influence of Luminescent Properties of Powders on the Fabrication of Scintillation Ceramics by Stereolithography 3D Printing. *Ceramics* **2023**, *6*, 43–57. [CrossRef]

25. Fedorov, A.A.; Dubov, V.V.; Ermakova, L.V.; Bondarev, A.G.; Karpyuk, P.V.; Korzhik, M.V.; Kuznetsova, D.E.; Mechinsky, V.A.; Smyslova, V.G.; Dosovitskiy, G.A.; et al. $Gd_3Al_2Ga_3O_{12}$:Ce Scintillation Ceramic Elements for Measuring Ionizing Radiation in Gases and Liquids. *Instrum. Exp. Tech.* **2023**, *66*, 234–238. [CrossRef]

26. Karipbayev, Z.T.; Lisitsyn, V.M.; Mussakhanov, D.A.; Alpyssova, G.K.; Popov, A.I.; Polisadova, E.F.; Elsts, E.; Akilbekov, A.T.; Kukenova, A.B.; Kemere, M.; et al. Time-resolved luminescence of YAG:Ce and YAGG:Ce ceramics prepared by electron beam assisted synthesis. *Nucl. Instrum. Meth. B* **2020**, *479*, 222–228. [CrossRef]

27. Abd, H.R.; Hassan, Z.; Ahmed, N.M.; Omar, A.F.; Thahab, S.M.; Lau, K.S. Rapid synthesis of Ce^{3+}:YAG via CO_2 laser irradiation combustion method: Influence of Ce doping and thickness of phosphor ceramic on the performance of a white LED device. *J. Solid State Chem.* **2021**, *294*, 121866. [CrossRef]

28. Loiko, P.; Basyrova, L.; Maksimov, R.; Shitov, V.; Baranov, M.; Starecki, F.; Mateos, X.; Camy, P. Comparative study of Ho:Y_2O_3 and Ho:$Y_3Al_5O_{12}$ transparent ceramics produced from laser-ablated nanoparticles. *J. Lumin.* **2021**, *240*, 118460. [CrossRef]

29. Timoshenko, A.D.; Matvienko, O.O.; Doroshenko, A.G.; Parkhomenko, S.V.; Voronova, I.O.; Kryzhanovska, O.S.; Safronova, N.A.; Vovk, O.O.; Tolmachev, A.V.; Baumer, V.N.; et al. Highly-doped YAG:Sm^{3+} transparent ceramics: Effect of Sm^{3+} ions concentration. *Ceram. Int.* **2023**, *49*, 7524–7533. [CrossRef]

30. Wagner, A.; Ratzker, B.; Kalabukhov, S.; Kolusheva, S.; Sokol, M.; Frage, N. Highly-doped Nd:YAG ceramics fabricated by conventional and high pressure SPS. *Ceram. Int.* **2019**, *45*, 12279–12284. [CrossRef]

31. Derdzyan, M.V.; Hovhannesyan, K.L.; Santos, S.N.C.; Dujardin, C.; Petrosyan, A.G. Influence of Air Annealing on Optical and Scintillation Properties of YAG:Pr,Ca. *Phys. Status Solidi A* **2022**, *220*, 2200571. [CrossRef]

32. Kuznetsova, D.E.; Volkov, P.A.; Dosovitskiy, G.A.; Mikhlin, A.L.; Bogatov, K.B.; Retivov, V.M.; Dosovitskiy, A.E. Influence of alkali metal impurities on properties of yttrium aluminum garnet doped with cerium. *Russ. Chem. Bull.* **2016**, *65*, 1734–1738. [CrossRef]

33. Karpyuk, P.; Shurkina, A.; Kuznetsova, D.; Smyslova, V.; Dubov, V.; Dosovitskiy, G.; Korzhik, M.; Retivov, V.; Bondarev, A. Effect of Sintering Additives on the Sintering and Spectral-Luminescent Characteristics of Quaternary GYAGG:Ce Scintillation Ceramics. *J. Electron. Mater.* **2022**, *51*, 6481–6491. [CrossRef]

34. Vorona, I.O.; Yavetskiy, R.P.; Parkhomenko, S.V.; Doroshenko, A.G.; Kryzhanovska, O.S.; Safronova, N.A.; Timoshenko, A.D.; Balabanov, A.E.; Tolmachev, A.V.; Baumer, V.N. Effect of complex $Si^{4+}+Mg^{2+}$ additive on sintering and properties of undoped YAG ceramics. *J. Eur. Ceram. Soc.* **2022**, *42*, 6104–6109. [CrossRef]

35. Setlur, A.A.; Heward, W.J.; Hannah, M.E.; Happek, U. Incorporation of Si^{4+}–N^{3-} into Ce^{3+}-Doped Garnets for Warm White LED Phosphors. *Chem. Mater.* **2008**, *20*, 6277–6283. [CrossRef]

36. Dosovitskii, G.A.; Bogatov, K.B.; Volkov, P.A.; Mikhlin, A.L.; Dosovitskii, A.E. Effect of adding boron on morphological and functional properties of aluminum-yttrium garnet activated with europium. *Refract. Ind. Ceram.* **2013**, *54*, 69–73. [CrossRef]

37. Yan, Y.; Meshbah, A.; Kheouz, L.; Bouillet, C.; Lorentz, C.; Blanchard, N.; Berends, A.C.; van der Haar, M.A.; Lerouge, F.; Krames, M.R.; et al. Ultra-Small YPO_4-YAG:Ce Composite Nanophosphors with a Photoluminescence Quantum Yield Exceeding 50%. *Small* **2023**, *19*, 2208055. [CrossRef]

38. Pirrung, F.O.H.; Noordam, A.; Harbers, P.J.; Loen, E.M.; Munneke, A.E. Phosphoric Acid Esters and Their Use as Wetting and Dispersing Agent. US Patent 7595416B2, 28 February 2005. Available online: https://patents.google.com/patent/US7595416B2/ (accessed on 5 July 2023).

39. Gobelt, B.; Nagelsdiek, R.; Omeis, J.; Piestert, F.; Pritschins, W.; Meznaric, N.; Schroder, D.; Tiegs, W. Dispersing Additives Based on Phosphoric Acid Ester Derivatives. US Patent 9518146, 4 May 2012. Available online: https://patents.google.com/patent/US9518146B2 (accessed on 5 July 2023).

40. Gordienko, E.; Fedorov, A.; Radiuk, E.; Mechinsky, V.; Dosovitskiy, G.; Vashchenkova, E.; Kuznetsova, D.; Retivov, V.; Dosovitskiy, A.; Korjik, M.; et al. Synthesis of crystalline Ce-activated garnet phosphor powders and technique to characterize their scintillation light yield. *Opt. Mater.* **2018**, *78*, 312–318. [CrossRef]

41. Pardo, A.; Romero, J.; Ortiz, E. High-temperature behaviour of ammonium dihydrogen phosphate. *J. Phys. Conf. Ser.* **2017**, *935*, 012050. [CrossRef]

42. Su, C.H.; Chen, C.C.; Liaw, H.J.; Wang, S.C. The Assessment of Fire Suppression Capability for the Ammonium Dihydrogen Phosphate Dry Powder of Commercial Fire Extinguishers. *Procedia Eng.* **2014**, *84*, 485–490. [CrossRef]

43. Li, X.; Wang, H.; Guan, L.; Fu, Y.; Guo, Z.; Yuan, K.; Tie, L.; Yang, Z.; Teng, F. Influence of pH value on properties of YPO_4:Tb^{3+} phosphor by co-precipitation method. *J. Rare Earths* **2015**, *33*, 346–349. [CrossRef]

44. Li, J.; Zhu, J.; Li, P.; Nan, C.; Zhang, Y. Roles of $(NH_4)_2HPO_4$ and $NH_4H_2PO_4$ in the phase transition and luminescence enhancement of YPO_4:Eu. *J. Phys. Chem. Solids* **2021**, *150*, 109821. [CrossRef]

45. Agrawal, D.; Hummel, F.A. The Systems Y_2O_3-P_2O_5 and Gd_2O_3-P_2O_5. *J. Electrochem. Soc.* **1980**, *127*, 1550. [CrossRef]

46. Szuszkiewicz, W.; Znamierowska, T. Y_2O_3-P_2O_5 Phase Diagram. *Pol. J. Chem.* **1989**, *63*, 381–391.

47. Grew, E.S.; Locock, A.J.; Mills, S.J.; Galuskina, I.O.; Galuskin, E.V.; Halenius, U. Nomenclature of the garnet supergroup. *Am. Miner.* **2013**, *88*, 785–811. [CrossRef]

48. Thompson, R.N. Is upper-mantle phosphorus contained in sodic garnet? *Earth Planet Sci. Lett.* **1975**, *26*, 417–424. [CrossRef]

49. Brunet, F.; Bonneau, V.; Irifune, T. Complete solid-solution between $Na_3Al_2(PO_4)_3$ and $Mg_3Al_2(SiO_4)_3$ garnets at high pressure. *Am. Mineral.* **2006**, *91*, 211–215. [CrossRef]